DEVELOPMENTAL NEUROSCIENCE

Localized astrogenesis regulates gyrification of the cerebral cortex

Yohei Shinmyo[1]*†, Kengo Saito[1]†, Toshihide Hamabe-Horiike[1], Narufumi Kameya[1], Akitaka Ando[1], Kanji Kawasaki[1], Tung Anh Dinh Duong[1], Masataka Sakashita[1], Jureepon Roboon[2], Tsuyoshi Hattori[2], Takayuki Kannon[3], Kazuyoshi Hosomichi[3], Michal Slezak[4,5], Matthew G. Holt[4,6], Atsushi Tajima[3], Osamu Hori[2], Hiroshi Kawasaki[1]*

The development and evolution of mammalian higher cognition are represented by gyrification of the laminar cerebral cortex and astrocyte development, but their mechanisms and interrelationships remain unknown. Here, we show that localized astrogenesis plays an important role in gyri formation in the gyrencephalic cerebral cortex. In functional genetic experiments, we show that reducing astrocyte number prevents gyri formation in the ferret cortex, while increasing astrocyte number in mice, which do not have cortical folds, can induce gyrus-like protrusions. Morphometric analyses demonstrate that the vertical expansion of deep pallial regions achieved by localized astrogenesis is crucial for gyri formation. Furthermore, our findings suggest that localized astrogenesis by a positive feedback loop of FGF signaling is an important mechanism underlying cortical folding in gyrencephalic mammalian brains. Our findings reveal both the cellular mechanisms and the mechanical principle of gyrification in the mammalian brain.

INTRODUCTION

During mammalian evolution, the cerebral cortex has changed markedly, resulting in the acquisition of higher cognitive functions (*1*–*7*). Notable changes during evolution include the expansion and folding (i.e., gyrification) of the cerebral cortex. Because malformations of cortical folds in human patients, such as lissencephaly and polymicrogyria, are associated with severe intellectual disability and epilepsy, folding of the cerebral cortex is considered to be indispensable for higher brain functions (*8*–*12*). Therefore, investigation of molecular and cellular mechanisms underlying cortical folding is critical for understanding not only the evolution of the mammalian cerebral cortex but also the pathogenesis of human cortical malformations. However, our understanding of the mechanisms underlying cortical folding is still rudimentary.

In addition to neurons, glial cells have markedly increased with brain expansion during evolution (*13*). Astrocytes, one type of glial cell, play a range of crucial roles such as modulation of synaptic functions, maintenance of extracellular ion balance, and provision of nutrients to neurons (*14*–*18*). By contacting the nodes of Ranvier, astrocytes also participate in remodeling myelin structures, which influence the conduction velocities of axons (*19*). Furthermore, astrocyte dysfunction is involved in various neurological and neurodevelopmental diseases (*20*). A previous study showed that mice that have human astrocytes exhibited improved cognitive abilities, suggesting that astrocytes themselves have also changed during evolution (*21*). Thus, astrocytes are increasingly appreciated as important contributors to higher brain functions.

To investigate the mechanisms underlying the development and evolution of the cerebral cortex, carnivore ferrets have attracted attention as an important model animal (*22*–*26*). This is because ferrets have gyrencephalic brains, and genetic manipulation techniques for ferrets have been established (*27*–*30*). Using ferrets, previous studies have uncovered neuronal processes involved in the development and evolution of the cerebral cortex (*25*–*27*, *30*–*32*). Here, we propose a novel two-step model of gyrification of the cerebral cortex. We established genetic manipulation techniques for astrocytes in the cerebral cortex by combining in utero electroporation (IUE) and the *piggyBac* system and found that a marked expansion of astrocytes in restricted areas within gyri in the ferret cortex was mediated by a positive feedback loop driven by fibroblast growth factor (FGF) signaling. The overproduction of astrocytes by activation of FGF signaling induced gyrus-like protrusions in the mouse cerebral cortex. Furthermore, we found that localized astrogenesis is indispensable for cortical folding in the ferret brain via its role in the vertical expansion of the deep pallial regions. Our findings reveal both the cellular mechanisms and the mechanical principle of gyrification in the mammalian brain.

RESULTS

Ferret astrogenesis is regulated by FGF signaling in an autocrine manner

We previously showed that FGF signaling is crucial for folding of the cerebral cortex in ferrets (*31*, *33*). We noticed that activation of FGF signaling increased not only layer 2/3 neurons but also astrocytes (*33*). This finding raised the possibility that FGF signaling might directly control the number of astrocytes during development. To test this possibility, we activated FGF signaling during astrogenesis in the developing mouse cerebral cortex by combining IUE, the $ER^{T2}CreER^{T2}$/loxP system, and the *piggyBac* system (fig. S1A). The activation of FGF signaling during astrogenesis induced

[1]Department of Medical Neuroscience, Graduate School of Medical Sciences, Kanazawa University, Ishikawa 920-8640, Japan. [2]Department of Neuroanatomy, Graduate School of Medical Sciences, Kanazawa University, Ishikawa 920-8640, Japan. [3]Department of Bioinformatics and Genomics, Graduate School of Advanced Preventive Medical Sciences, Kanazawa University, Ishikawa 920-8640, Japan. [4]VIB Center for Brain and Disease Research, Herestraat 49, Leuven 3000, Belgium. [5]Łukasiewicz Research Network-PORT Polish Institute for Technology Development, 54-066 Wroclaw, Poland. [6]Instituto de Investigação e Inovação em Saúde (i3S), University of Porto, 4200-135 Porto, Portugal.
*Corresponding author. Email: kawasaki@med.kanazawa-u.ac.jp (H.K.); shinmyo@med.kanazawa-u.ac.jp (Y.S.)
†These authors contributed equally to this work.

a drastic increase in S100β-positive astrocytes in mCherry-positive transfected regions of the cerebral cortex (fig. S1B, square brackets). Consistently, our quantification showed that the number of Sox9-positive and Sox10-negative astrocytes was significantly increased by the activation of FGF signaling (fig. S1C). In contrast, NeuN-positive neurons were not affected by the activation of FGF signaling (fig. S1, D and E). Double immunostaining for S100β and the cell proliferation marker Ki-67 showed that Ki-67– and S100β–double-positive cells were increased by the activation of FGF signaling (fig. S1, F and G). These results indicate that FGF signaling controls astrocyte number by regulating the proliferation of astrocytes in the developing cerebral cortex.

To identify endogenous FGF ligands regulating the proliferation of astrocytes, we first investigated the mRNA expression levels of FGF ligands in various cell types in the postnatal mouse cerebral cortex using transcriptome datasets reported previously (*34*). We found that, compared to other cell types in the mouse cerebral cortex, astrocytes had high expression levels of *Fgfs* (fig. S2), raising the possibility that FGF signaling regulates the proliferation of astrocytes in an autocrine manner. We next examined endogenous FGF ligands expressed in astrocytes in the ferret cerebral cortex, which has more astrocytes than the mouse cerebral cortex. To isolate astrocytes, we prepared primary cultures of astrocytes from the developing ferret cerebral cortex (Fig. 1A). We extracted RNA from cultured astrocytes and examined the mRNA expression levels of FGF ligands using an Illumina HiSeq 2000 platform. We found that *FGF1* and *FGF2* expression levels were markedly higher than those of the other FGF ligands, although *FGF2* levels were lower than *FGF1* levels (Fig. 1A). Double labeling with RNAscope in situ hybridization (ISH) and immunostaining for the astrocyte marker glutamine synthetase (GS) revealed that *FGF1* and *FGF2* were expressed in astrocytes in the ferret cerebral cortex (Fig. 1B). ISH for *FGF receptors* (*FGFRs*) and immunostaining for GS showed that *FGFR2* and *FGFR3* were predominantly expressed in astrocytes in the ferret cerebral cortex (Fig. 1C). These results suggest that FGF1 and FGF2 secreted from astrocytes function in an autocrine manner through FGFRs expressed in astrocytes.

To examine the roles of FGF1 or FGF2, we treated cultured ferret astrocytes with FGF1 or FGF2 protein (10 ng/ml) and found that Ki-67– and glial fibrillary acidic protein (GFAP)–double-positive cells were significantly increased in both cases (n = 3 animals for each condition; *P < 0.05, Welch's t test) (Fig. 1, D and E). Consistently, injection of FGF1 or FGF2 protein into the lateral ventricle of the neonatal mouse brain markedly increased the percentage of astrocytes coexpressing Ki-67 (fig. S3, A to C), suggesting that astrocyte proliferation is enhanced by FGF1 and FGF2 in the cerebral cortex. To determine whether the endogenous FGF ligands secreted by astrocytes were required for their proliferation, we treated cultured astrocytes with BGJ398, a potent pan-FGFR inhibitor. Our quantitative analysis showed that BGJ398 significantly reduced Ki-67–positive astrocytes [n = 4 animals for each condition; **P < 0.01; N.S., not significant, one-way analysis of variance (ANOVA) followed by Tukey's honestly significant difference (HSD) test] (Fig. 1, F and G). Together, our results uncovered a regulatory mechanism whereby FGFs secreted by astrocytes efficiently increase the number of astrocytes through a positive feedback loop.

Astrocyte number in the cerebral cortex has markedly increased during mammalian evolution, and it seemed plausible that the expression level of FGFs in astrocytes is a key determinant of astrocyte number across mammalian species. We therefore performed RNA-sequencing (RNA-seq) analysis of cultured astrocytes from the mouse cerebral cortex and compared the expression levels of *FGFs* in astrocytes between mice and ferrets. We found that the mRNA expression levels of *FGF1* in ferret astrocytes were much higher than those in mouse astrocytes, while those of *glyceraldehyde-3-phosphate dehydrogenase* (*GAPDH*) and *tyrosine 3-monooxygenase/tryptophan 5-monooxygenase activation protein zeta* (*YWHAZ*), which are commonly used as reference genes, were comparable between them (Fig. 1H). To compare *FGF1* expression levels in vivo, we performed RNAscope ISH for *FGF1* and immunostaining for GS using sections of the cerebral cortex. The number of *FGF1* puncta in ferret astrocytes was significantly larger than that in mouse astrocytes (n = 3 animals for each condition; **P < 0.01, Welch's t test) (Fig. 1, I and J). Consistently, another quantitative index, the H-score representing mRNA expression levels per cell, showed that *FGF1* expression in astrocytes in the ferret cerebral cortex was significantly higher than that in the mouse cerebral cortex (n = 3 animals for each condition; **P < 0.01, Welch's t test) (Fig. 1K). We further performed RNAscope ISH for *SPROUTY2* (*SPRY2*) and *Ets Variant Gene 5* (*ETV5*) to investigate the activation of FGF signaling in astrocytes in the postnatal ferret and mouse cerebral cortices. We found that expression of both *SPRY2* and *ETV5* in astrocytes was significantly higher in the ferret cerebral cortex than in the mouse cerebral cortex (n = 3 animals for each condition; **P < 0.01, Welch's t test) (Fig. 1, L and M, and fig. S3, D to F). These results indicate that FGF signaling is more activated in ferret astrocytes than in mouse astrocytes in the postnatal cerebral cortex.

Last, to examine whether FGF1 increases the number of astrocytes in vivo, we expressed FGF1 in the mouse cerebral cortex during astrogenesis by combining IUE, the $ER^{T2}CreER^{T2}$/loxP system, and the *piggyBac* system. We found that FGF1 markedly increased astrocytes in the cerebral cortex (fig. S3, G and H), while it did not affect the number of neurons (fig. S3, I and J). Our results indicate that changes in *FGF1* expression were, at least in part, responsible for the increases in astrocytes in the cerebral cortex that occurred during mammalian evolution.

FGF signaling is sufficient for producing folds on the lissencephalic mouse cerebral cortex

Another major change that occurred during evolution was the appearance of folds on the surface of the cerebral cortex, and the mechanisms of cortical folding have been of great interest (*1*, *2*, *7*, *12*). Although it has been proposed that cortical folding is mediated by neurogenesis, we noticed that cortical folding continues during astrogenesis in the ferret cerebral cortex. Furthermore, a recent study reported that progenitors in the subventricular zone (SVZ) produce glial cells during late developmental stages, coinciding with cortical folding in the macaque monkey (*35*). We therefore hypothesized that the increase in astrocytes during evolution contributed to the appearance of cortical folds. To test this hypothesis, we increased astrocytes in the lissencephalic mouse cerebral cortex by activating FGF signaling during astrogenesis (fig. S1). We found that gyrus-like protrusions formed on the surface of the mouse cerebral cortex (Fig. 2, A to C). Our quantitative analysis showed that activation of FGF signaling significantly induced the vertical expansion of the mouse cerebral cortex (n = 3 animals for each condition; **P < 0.01, Welch's t test) (Fig. 2D). When wide areas of the cerebral cortex were transfected, we often observed two protrusions and a hollow

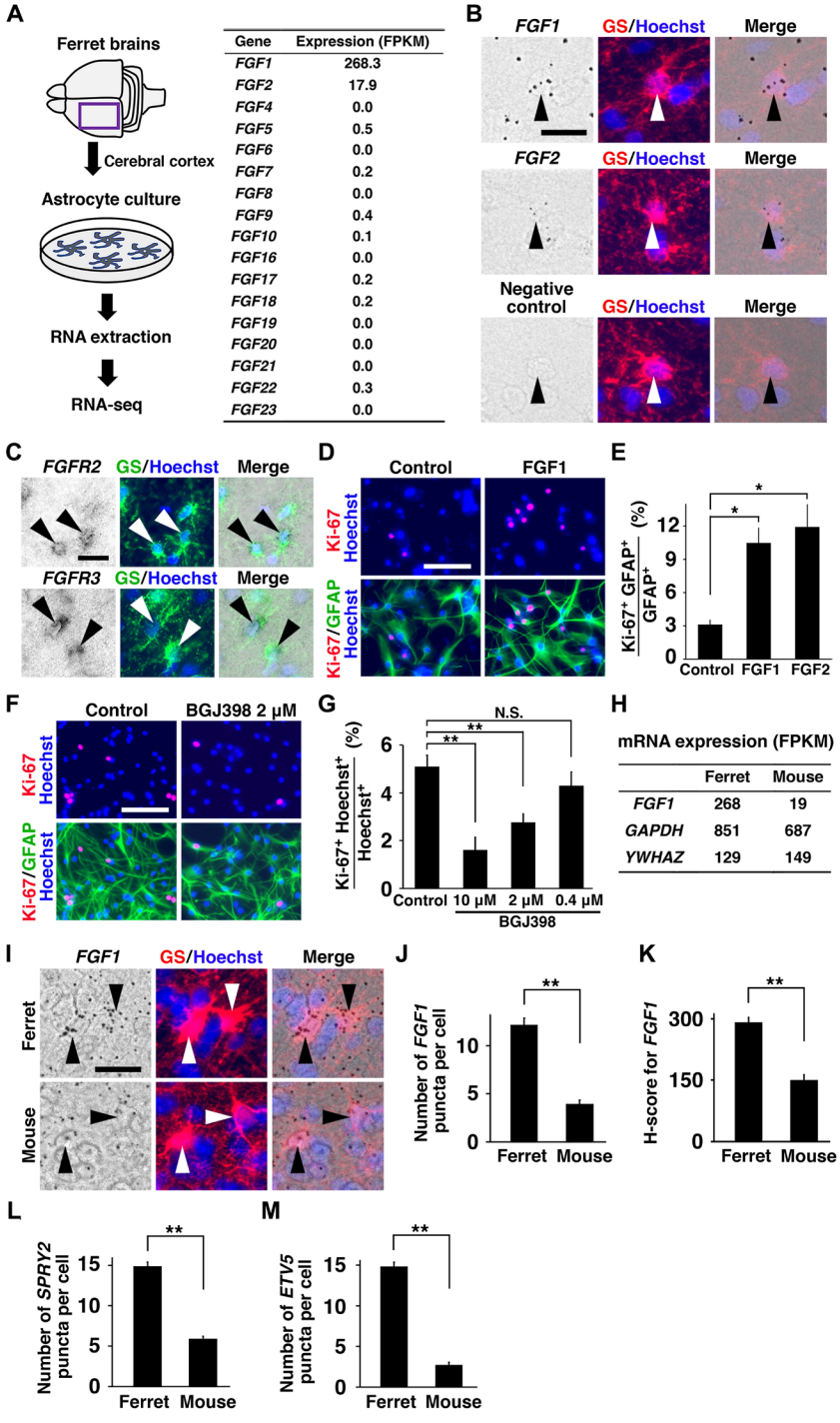

Fig. 1. FGF1 and FGF2 promote proliferation of astrocytes in an autocrine manner. (**A**) RNA was extracted from cultured ferret astrocytes and analyzed by RNA-seq. An expression profile of *FGF* ligands is shown. (**B**) Coronal sections of the ferret cortex at P16 were subjected to immunostaining with anti-GS antibody and RNAscope ISH for *FGF1* or *FGF2*. (**C**) Coronal sections of the ferret cortex at P16 were subjected to immunostaining with anti-GS antibody and ISH for *FGFR2* or *FGFR3*. (**D**) Astrocytes cultured with FGF1 or FGF2 protein were stained with anti–Ki-67 and anti-GFAP antibodies. (**E**) Percentages of GFAP-positive cells coexpressing Ki-67 in astrocytes cultured with FGF1, FGF2, or vehicle. (**F**) Astrocytes cultured with BGJ398 were stained with anti–Ki-67 and anti-GFAP antibodies. (**G**) Percentages of Hoechst-positive cells coexpressing Ki-67 in astrocytes cultured with BGJ398. (**H**) RNA was extracted from cultured ferret and mouse astrocytes and analyzed by RNA-seq. Expression levels of *FGF1*, *GAPDH*, and *YWHAZ* are shown. (**I** to **M**) Coronal sections of the ferret cortex at P36 and the mouse cortex at P18 were subjected to RNAscope ISH for *FGF1*, *SPRY2*, and *ETV5*, and immunostaining with anti-GS antibody. (I) High-magnification images of RNAscope ISH for *FGF1* and immunostaining for GS. Arrowheads indicate GS-positive astrocytes. (J, L, and M) Quantifications of the numbers of *FGF1* (J), *SPRY2* (L), and *ETV5* (M) puncta per an astrocyte in the cortex of ferrets and mice. (K) Quantification of the H-score for *FGF1* in the cortex of ferrets and mice. **P* < 0.05; ***P* < 0.01; N.S., not significant. All error bars represent means ± standard deviation. Scale bars, 20 μm (B, C, and I) and 100 μm (D and F).

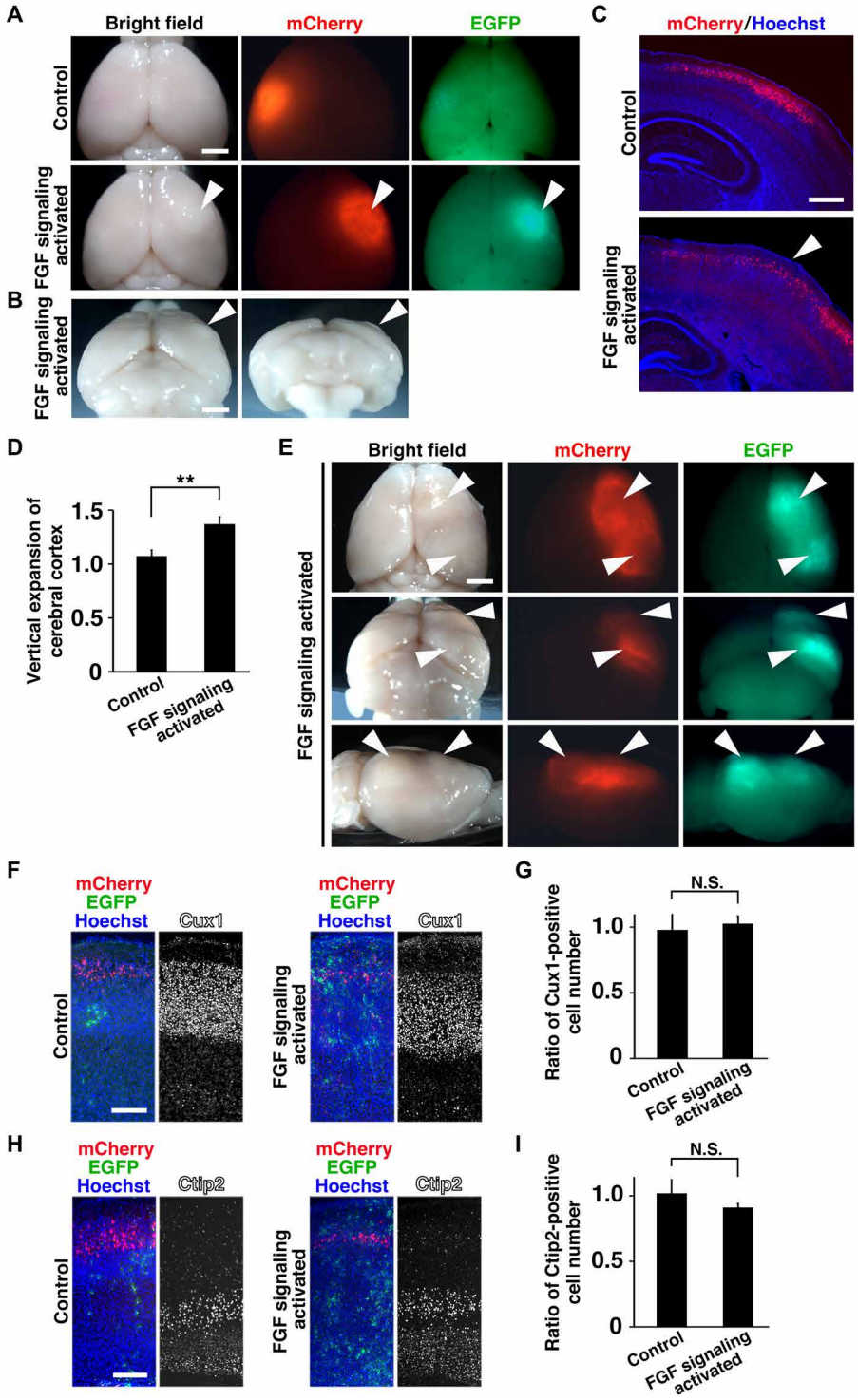

Fig. 2. Activation of FGF signaling induced gyrus-like structures in the mouse cerebral cortex. (**A** to **I**) pCAG-mCherry and pCAG-PBase plus either pPB-CAG-loxP-ER^{T2}CreER^{T2}-loxP-FGF8-IRES2-EGFP or the control plasmid were introduced into the mouse cortex at E15.5 using IUE. The pups were treated with 4-OHT three times (at P0, P1, and P2), and the brains were prepared at P10 (F to I) and P30 (A to E). (A) Dorsal views of the transfected brains. (B) Dorsoposterior (left) and posterior (right) views of the transfected brains. (C) Coronal sections of the brains were stained with Hoechst 33342. Note that a protrusion on the surface of the brains was induced by activation of FGF signaling [arrowheads in (A) to (C)]. (D) Quantification of the vertical expansion of the mouse cortex by the activation of FGF signaling. (E) Dorsal (top), dorsoposterior (middle), and lateral (bottom) views of P30 brains with a wide transfected region. Note the two protrusions (arrowheads) and the hollow between them on the surface of the cortex. (F to I) Coronal sections of the cortex were stained with either anti-Cux1 antibody (F) or anti-Ctip2 antibody (H). Quantification of the numbers of Cux1-positive cells in layers 2 to 4 (G) and Ctip2-positive cells in layer 5 (I). The ratios of the numbers on the electroporated side to those on the non-electroporated side are shown. $^{**}P < 0.01$. All error bars represent means ± standard deviation. Scale bars, 2 mm (A, B, and E), 0.5 mm (C), and 0.2 mm (F and H).

between them (Fig. 2E). The activation of FGF signaling increased astrocytes (fig. S1B) and did not affect cortical layer structure (Fig. 2, F and H) or the number of cortical neurons ($n = 3$ animals for each condition; N.S., Welch's t test) (Fig. 2, G and I). Consistently, in coronal sections, Hoechst staining and mCherry signals, which indicate transfected layer 2/3 neurons, revealed that the layer structure of the cerebral cortex was well preserved (Fig. 2C), suggesting that protrusions induced in the mouse cerebral cortex share properties similar to those in the gyrencephalic cerebral cortex. These results indicate that an increase in astrocytes is sufficient to induce gyrus-like protrusions in the lissencephalic cerebral cortex. It should be noted that the protrusions induced in the mouse cerebral cortex are milder than those observed in the gyrencephalic ferret cerebral cortex. This is presumably because the mechanisms of gyrification are not fully understood, and the incorporation of additional mechanisms would be necessary to make complete gyrus-like structures in the mouse cerebral cortex.

The mechanical processes producing cortical folds

We next investigated the mechanical processes producing protrusions and convolutions of cortical folds. Ferrets are born with a completely smooth cerebral cortex, and cortical folds are largely formed by postnatal day 16 (P16) (Fig. 3A). We measured the cortical thickness in the gyral crown of the suprasylvian gyrus (SSG) and those in the sulcal bottoms of the lateral sulcus (LS) and the suprasylvian sulcus (SSS) at P6, P10, and P16. Our quantitative analysis uncovered that vertical expansion of the subplate (SP)/intermediate zone (IZ) plus the outer SVZ (SP-OSVZ), rather than that of the cortical plate (CP) of gyri, is a prominent feature of cortical folding ($n = 4$ animals for P6, $n = 3$ animals for P10 and P16; $^{**}P < 0.01$; N.S., one-way ANOVA followed by Tukey's HSD test) (Fig. 3B and fig. S4). This observation led us to hypothesize that a vertical expansion of the SP and the prospective white matter (hereafter referred to as the deep pallial region) is an important mechanism of cortical folding.

Because it seemed plausible that the increase in astrocytes underlies the vertical expansion of the deep pallial regions, we next examined the distribution patterns of astrocytes in the ferret cerebral cortex using immunohistochemistry for the astrocyte markers S100β and GFAP. GFAP signals were mainly present in the SP/IZ and were more abundant in gyri than in sulci (Fig. 3C). S100β was distributed preferentially in the lower CP and the SP/IZ, and the number of S100β-positive cells was much greater in gyri than in sulci (Fig. 3D). These results are consistent with the idea that astrogenesis participates in cortical folding through the vertical expansion of the deep pallial regions in gyri. In addition, we performed ISH for *proteolipid protein* (*PLP*), which is a marker for mature oligodendrocytes. In contrast to GFAP and S100β signals, *PLP* signals were not abundantly present in the SP/IZ of gyri (fig. S5). Together, these results suggest that astrogenesis, rather than oligodendrogenesis, correlates with the vertical expansion of the deep pallial regions in gyri and with cortical folding.

We next examined whether FGF signaling is required for astrogenesis and vertical expansion in gyri by introducing dominant-negative FGFR, which is a soluble extracellular region of FGFR3 (sFGFR3) (*31*). Consistent with our previous report (*31*), when sFGFR3 was introduced, cortical folding was severely impaired, and the number of cortical neurons was reduced (Fig. 3E and fig. S6, A and B), suggesting that FGF signaling was efficiently suppressed in these samples. Immunostaining for S100β revealed that the number of astrocytes was markedly decreased by sFGFR3 (control, 1.02 ± 0.01; sFGFR3, 0.69 ± 0.16; $n = 3$ animals for control and $n = 4$ for sFGFR3; $^{*}P < 0.05$, Welch's t test) (Fig. 3, E and F). Furthermore, we found that sFGFR3 significantly reduced the vertical expansion of the SP-OSVZ in gyri (control, 0.84 ± 0.08; sFGFR3, 0.29 ± 0.10; $n = 3$ animals for each condition; $^{**}P < 0.01$, Welch's t test) (Fig. 3G). To confirm whether FGF signaling in astrocytes is suppressed by sFGFR3, we examined the expression of *ETV5* using RNAscope ISH. We found that the expression of *ETV5* mRNA in astrocytes was greatly reduced by sFGFR3 ($n = 3$ animals for each condition; $^{**}P < 0.01$, Welch's t test) (Fig. 3, H and I), showing that sFGFR3 suppresses FGF signaling in astrocytes. These results indicate that FGF signaling is required for astrogenesis and the vertical expansion of the deep pallial regions in gyri.

In addition, because we previously reported that upper layers of the cerebral cortex were preferentially reduced by sFGFR3 (*31*), we quantified NeuN signals in upper (layers 2 to 4) and lower (layers 5 and 6) layers of the cerebral cortex. Consistent with our previous observation (*31*), our quantification revealed that neurons in upper layers were predominantly reduced by sFGFR3 (fig. S6C). We also quantified S100β-positive cells in upper and lower layers of the cerebral cortex. In contrast with its effect in neurons, sFGFR3 caused a decrease in the number of S100β-positive astrocytes in both upper and lower layers (fig. S6D). Together with our previous study showing that preferential expansion of upper layers is involved in cortical folding (*31*), these results raised the possibility that FGF signaling mediates cortical folding by regulating both neurons and astrocytes.

Localized astrogenesis, via its role in the expansion of the deep pallial regions, is crucial for cortical folding

To further investigate the importance of astrogenesis for cortical folding, we attempted to inhibit astrogenesis in ferrets by blocking retinoic acid (RA) signaling because RA is known to facilitate astrocyte production in mice (*36*). We subcutaneously administered a pan-RA receptor antagonist, AGN 193109, into newborn ferrets from P3 to P15 (Fig. 4A). We found that cortical folds were severely reduced, and the surface of the brain became smoother in AGN 193109–treated pups (Fig. 4B). Hoechst staining of coronal sections revealed that AGN 193109 markedly reduced the sizes of gyri (arrow) and the depths of sulci (arrowhead) (Fig. 4C). Consistent with our observations, the local gyrus size (GYS) of the SSG (Fig. 4D) and the local sulcus depth (SD) of the LS (Fig. 4E) were significantly smaller in AGN 193109–treated cortex (local GYS; control, 2.91 ± 0.26 mm^2; AGN 193109, 1.47 ± 0.22 mm^2; $n = 4$ animals for control and $n = 3$ for AGN 193109; $^{*}P < 0.05$, Welch's t test) (local SD; control, 0.51 ± 0.07 mm; AGN 193109, 0.17 ± 0.03 mm; $n = 4$ animals for control and $n = 3$ for AGN 193109; $^{*}P < 0.05$, Welch's t test). These results indicate that AGN 193109 treatment during astrogenesis impaired cortical folding. We next investigated whether astrogenesis is affected by AGN 193109 treatment. Immunostaining showed that the GFAP-positive area in gyri was significantly reduced by AGN 193109 (control, 7.06 ± 0.60; AGN 193109, 3.33 ± 1.04; $n = 4$ animals for control and $n = 3$ for AGN 193109; $^{*}P < 0.05$, Welch's t test) (Fig. 4, F and H). Consistently, the number of S100β-positive astrocytes in gyri was also decreased by AGN 193109 (control, 12.2 ± 1.9; AGN 193109, 4.06 ± 0.76; $n = 4$ animals for control and $n = 3$ for AGN 193109; $^{**}P < 0.01$, Welch's t test) (Fig. 4, G and I). By contrast, the generation of cortical neurons was not predictably affected

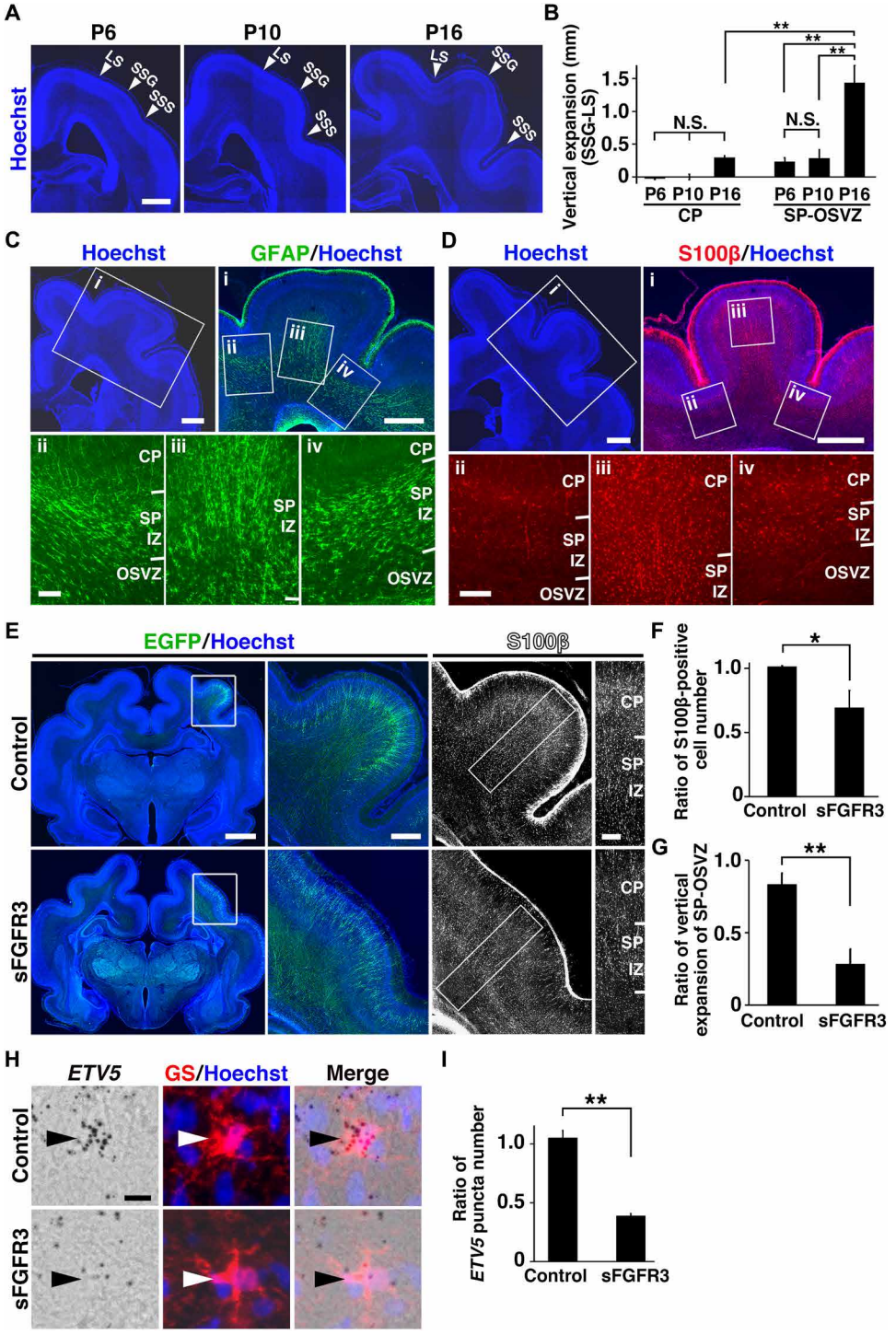

Fig. 3. FGF signaling is necessary for astrogenesis and cortical folding. (**A**) Coronal sections of ferret brains at P6, P10, and P16 were stained with Hoechst 33342. (**B**) Quantification of the vertical expansion of the SSG compared with the LS. (**C** and **D**) Coronal sections stained with either anti-GFAP antibody (C) or anti-S100β antibody at P16 (D). The areas within the boxes were magnified and are shown on the right and below. (**E** to **I**) pCAG-EGFP plus either pCAG-sFGFR3 or control vector were introduced into the ferret cortex at E33, and the brains were prepared at P6 (H and I) and P16 (E to G). Coronal sections were stained with anti-GFP and anti-S100β antibodies. The areas within the boxes in the left panels were magnified and are shown in the middle panels. Images of S100β staining corresponding to the areas within the boxes are shown on the right. Further magnified images of S100β staining within the boxed areas are shown on the far right. (F) Effect of sFGFR3 on the S100β-positive cell number in the SSG. (G) Effect of sFGFR3 on the vertical expansion of the SP-OSVZ. (H) Coronal sections were subjected to *ETV5* RNAscope ISH and GS immunostaining. High-magnification images of astrocytes (arrowheads) are shown. (I) Effect of sFGFR3 on the number of *ETV5* puncta in astrocytes. $^{*}P < 0.05$; $^{**}P < 0.01$. All error bars represent means ± standard deviation. Scale bars, 1 mm (A; C, top; D, top), 0.2 mm (C, bottom; D, bottom; E, rightmost), 2 mm (E, left), 0.5 mm (E, middle), and 20 μm (H). LS, lateral sulcus; SSG, suprasylvian gyrus; SSS, suprasylvian sulcus; CP, cortical plate; SP, subplate; IZ, intermediate zone; OSVZ, outer subventricular zone.

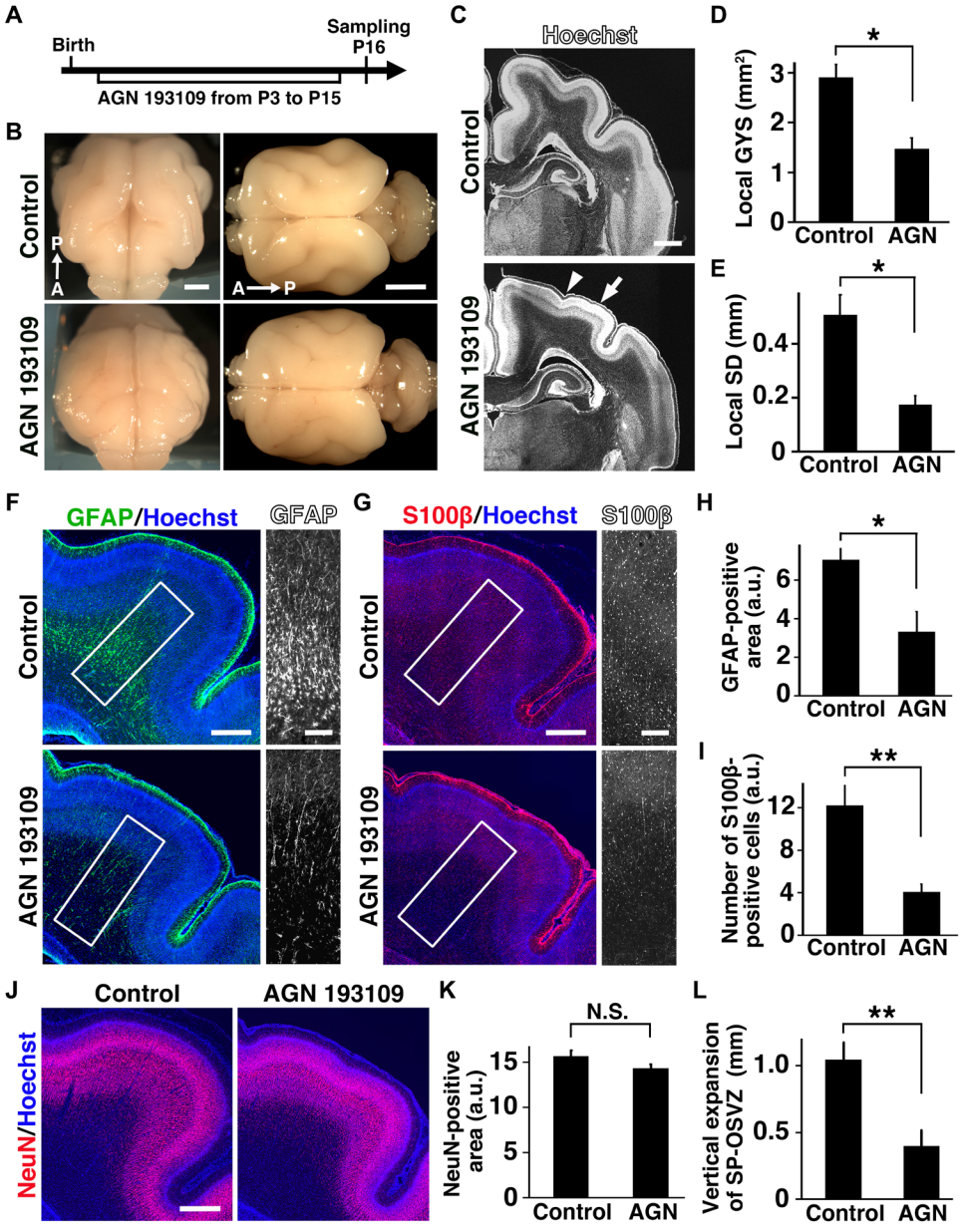

Fig. 4. Inhibition of astrogenesis impaired vertical expansion in gyri and cortical folding. (**A**) Experimental procedure for AGN 193109 treatment for ferret pups. AGN 193109 was introduced by daily subcutaneous injections from P3 to P15, and the brains were prepared at P16. (**B**) Dorsoanterior (left) and dorsal (right) views of the brains at P16. (**C**) Coronal sections of the brains were stained with Hoechst 33342. Note that the depths of sulci (arrowhead) and the sizes of gyri (arrow) were markedly reduced by AGN 193109. (**D** and **E**) Quantification of the local GYS of the SSG (D) and the local SD of the LS (E). (**F** and **G**) Coronal sections stained with either anti-GFAP (F) or anti-S100β antibody (G). GFAP and S100β images within the boxed areas in the left panels were magnified and are shown on the right. (**H** and **I**) Quantification of the GFAP-positive area (H) and the S100β-positive cell number (I) in the SSG. (**J**) Coronal sections stained with anti-NeuN antibody. (**K**) Quantification of NeuN-positive areas in the SSG of the cortex from control and AGN 193109–treated pups. (**L**) Quantification of the vertical expansion of the deep pallial region in the SSG. The length of the SP-OSVZ in the LS was subtracted from that in the SSG. $^{*}P < 0.05$; $^{**}P < 0.01$. Error bars in (D) and (E) represent means ± standard error of the mean and those in (H), (I), (K), and (L) represent means ± standard deviation. Scale bars, 4 mm (B), 1 mm (C), 0.5 mm (F, left; G, left; J), and 0.2 mm (F, right; G, right). A, anterior; P, posterior; a.u., arbitrary units.

by AGN 193109 treatment (control, 15.6 ± 0.65; AGN 193109, 14.3 ± 0.42; $n = 3$ for each condition; N.S., Welch's t test) (Fig. 4, J and K). In addition, immunostaining for Satb2 and Ctip2 showed that cortical layer structures were not affected by AGN 193109 treatment (fig. S7). The vertical expansion of the SP-OSVZ in gyri was significantly reduced by AGN 193109 (control, 1.04 ± 0.13 mm; AGN 193109, 0.40 ± 0.12 mm; $n = 3$ for each condition; $^{**}P < 0.01$, Welch's t test) (Fig. 4L). These results are consistent with the idea that inhibition of RA signaling during astrogenesis suppressed the generation of astrocytes, resulting in the reduced vertical expansion of the deep pallial regions and impairment of cortical folding.

To directly demonstrate that astrocytes are required for cortical folding, we tried to selectively eliminate astrocytes in the ferret cerebral cortex. We performed IUE to introduce the *piggyBac*

transposon plasmid system, in which the expression of diphtheria toxin A (DTA) fragment was driven by the human GFAP promoter (named gfa2 promoter) (*37*). First, we characterized the transgene expression driven by the gfa2 promoter in the ferret cerebral cortex. Using IUE at embryonic day 31 (E31), we introduced the donor plasmid pPB-gfa2-EGFP, the helper plasmid pCAG-PBase, and episomal pCAG-mCherry, which served as transfection control, and the brains were prepared at P16. We found that enhanced green fluorescent protein (EGFP) driven by the gfa2 promoter was broadly distributed including in the CP, the SP/IZ, and the OSVZ, while mCherry-positive neurons were mainly restricted to the lower CP (Fig. 5A). Immunostaining and ISH with cell type–specific markers revealed that the *piggyBac* system with the gfa2 promoter selectively induced transgene expression in astrocytes in the ferret cerebral cortex (fig. S8, A to D). We further examined whether this plasmid induces transgene expression in the germinal zone of the ferret cerebral cortex at E36. pPB-gfa2-EGFP rarely induced EGFP signals in the ventricular zone (VZ) (fig. S8, E and F). In contrast, pPB-CAG-EGFP induced strong EGFP expression in many cells in the VZ (fig. S8, E and F). Both pPB-gfa2-EGFP and pPB-CAG-EGFP induced strong EGFP expression in astrocytes (fig. S8G).

To test whether the donor plasmid pPB-gfa2-DTA is useful for eliminating astrocytes, we electroporated two donor plasmids, pPB-gfa2-EGFP and pPB-gfa2-DTA, with the helper plasmid into the mouse cerebral cortex at E15.5 (fig. S9A). Our quantification showed that EGFP-positive astrocytes were greatly reduced by pPB-gfa2-DTA, whereas the number of mCherry-positive neurons was not affected (fig. S9, B to D). This result indicates that pPB-gfa2-DTA is useful for selectively eliminating astrocytes in the cerebral cortex. We then eliminated astrocytes in the ferret cerebral cortex using IUE and pPB-gfa2-DTA at E31, and the brains were prepared at P16 (Fig. 5B). We found severe impairments in cortical folding in the DTA-transfected cortex, while no apparent abnormalities were observed in the control cortex transfected with pPB-gfa2-EGFP (Fig. 5C). Coronal sections showed remarkable reductions in the sizes of gyri (Fig. 5D, arrow) and the depths of sulci (Fig. 5D, arrowhead) in the DTA-transfected side of the cortex compared with the contralateral side of the cortex (Fig. 5D). The local GYS ratio (Fig. 5E) and the local SD ratio (Fig. 5F) were significantly smaller in the DTA-transfected cortex than in the control cortex (local GYS ratio; control, 0.95 ± 0.07; DTA, 0.47 ± 0.02; $n = 3$ animals for control and $n = 4$ for DTA; $^{*}P < 0.05$, Welch's t test) (local SD ratio; control, 0.90 ± 0.06; DTA, 0.35 ± 0.07; $n = 3$ animals for control and $n = 4$ for DTA; $^{**}P < 0.01$, Welch's t test).

We next morphometrically investigated the vertical expansion in gyri. We found a significant reduction in the vertical expansion of the SP-OSVZ of the DTA-transfected cortex (control, 0.86 ± 0.06; DTA, 0.28 ± 0.03; $n = 3$ for each condition; $^{**}P < 0.01$, Welch's t test) (Fig. 5G). Furthermore, S100β-positive cells in gyri of the DTA-transfected cortex were significantly decreased (control, 1.14 ± 0.17; DTA, 0.59 ± 0.15; $n = 3$ animals for each condition; $^{*}P < 0.05$, Welch's t test) (Fig. 5, H to J), while there was no significant difference in the density of S100β-positive cells between the DTA-transfected cortex and the control cortex (control, 0.98 ± 0.20; DTA, 0.80 ± 0.25; $n = 3$ animals for each condition; N.S., Welch's t test) (Fig. 5, H, I, and K). Similarly, the GFAP-positive area in gyri of the DTA-transfected cortex was significantly smaller than that of the control cortex (control, 1.21 ± 0.25; DTA, 0.49 ± 0.03; $n = 4$ animals for control and $n = 3$ for DTA; $^{*}P < 0.05$, Welch's t test) (Fig. 5L and fig. S10A), although GFAP signal density in gyri of the DTA-transfected cortex was not significantly reduced (control, 1.12 ± 0.26; DTA, 0.79 ± 0.05; $n = 4$ animals for control and $n = 3$ for DTA; N.S., Welch's t test) (Fig. 5M and fig. S10A). We did not observe obvious defects in generation and lamination of cortical neurons in the DTA-transfected brain (control, 0.92 ± 0.09; DTA, 1.06 ± 0.09; $n = 3$ for each condition; N.S., Welch's t test) (Fig. 5N and fig. S10B). These results indicate that astrocytes were selectively eliminated by expressing DTA in the ferret cerebral cortex, and our findings demonstrate a crucial role of astrocytes in cortical folding.

DISCUSSION

Both an increase in astrocytes and the appearance of cortical folds are prominent features of the cerebral cortex that emerged during mammalian evolution. Here, we have shown that localized astrogenesis is indispensable for cortical folding through the vertical expansion of the deep pallial regions in the gyrencephalic brain of ferrets. Furthermore, our data suggest that a positive feedback loop driven by FGF signaling contributes to an increase in astrocyte number in the cerebral cortex of gyrencephalic brains.

Numerous studies have shown that gyrencephalic animals including humans, monkeys, and ferrets have larger amounts of neural progenitors in the SVZ (*38*–*42*). We previously demonstrated that neural progenitors in the SVZ are required for the production of upper-layer neurons necessary for cortical folding in ferrets (*31*). It was recently shown that the human-specific gene *ARHGAP11B* promotes the production of upper-layer neurons and cortical folding by regulating the number of neural progenitors (*43*). Together with previous observations that cortical neurons migrate in a tangential orientation without following strict radial paths in the developing ferret brain (*44*, *45*), these results suggest that cortical folding requires a tangential expansion of the superficial cortical portion (*30*). In this study, we uncovered a mechanism underlying cortical folding, namely, the astrogenesis-mediated vertical expansion of the deep pallial regions in gyri. Presumably, the tangential expansion of the cortical surface mediates the initiation of cortical folding during early development, and this is followed by the vertical expansion of the deep pallial regions during astrogenesis, which results in fully developed cortical folds (Fig. 6). Our two-step model involving the cooperation between the tangential expansion of the cortical surface and the vertical expansion of the deep pallial regions seems to account well for the process of cortical folding.

Our findings suggest that a positive feedback loop of FGF signaling enables a marked expansion of astrocytes in restricted areas within gyri during the vertical expansion of the deep pallial regions. It is likely that FGF signaling has dual functions related to the local generation of astrocytes in the ferret cerebral cortex (Fig. 6). Initially, FGF signaling seems to control the generation of astrocytes from SVZ progenitors by regulating the proliferation of SVZ progenitors. FGFR-positive SVZ progenitors are more abundant in prospective gyral regions compared to prospective sulcal regions (*31*). Consistently, a previous study using monkeys revealed that SVZ progenitors were abundant in cortical regions where gyri will be formed (*46*). Furthermore, we previously reported that the proliferation of outer radial glial (RG) cells in the OSVZ was decreased by sFGFR3 in the developing ferret cerebral cortex, while the proliferation of RG cells in the VZ was not (*31*). It is therefore plausible that the abundance of SVZ progenitors in prospective gyral regions leads to

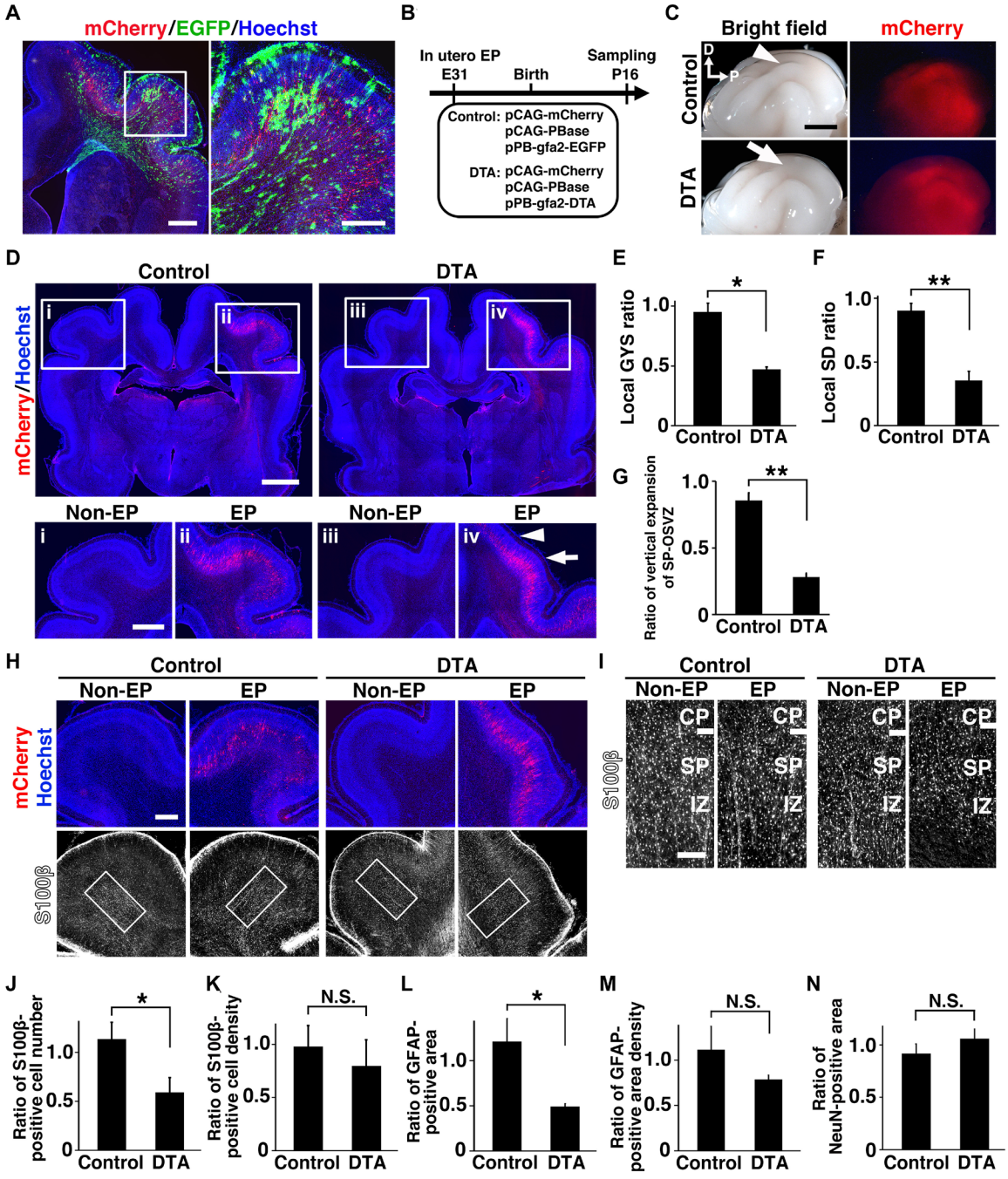

Fig. 5. Elimination of astrocytes led to reductions in vertical expansion in gyri and cortical folding. (**A**) pPB-gfa2-EGFP, pCAG-PBase, and pCAG-mCherry were introduced into the ferret cortex by IUE at E31. Coronal sections were prepared at P16 and stained with anti-GFP and anti-RFP antibodies. The area within the box was magnified and is shown on the right. (**B**) Experimental procedure for induction of DTA expression in astrocytes in the ferret cortex. (**C**) Lateral views of the electroporated brains at P16. Cortical folding was severely impaired by DTA expression (arrow), but not in the control brains (arrowhead). (**D**) Coronal sections stained with anti-RFP antibody. The areas within the boxes were magnified and are shown in the bottom panels. The depths of sulci (arrowhead) and the sizes of gyri (arrow) were markedly reduced by DTA. (**E** and **F**) Effects of DTA expression on the local GYS ratio (E) and the local SD ratio (F). (**G**) Quantification of vertical expansion of the deep pallial region. (**H** and **I**) Coronal sections stained with anti-RFP and anti-S100β antibodies. The areas within the boxes in (H) were magnified and are shown in (I). (**J** and **K**) Effects of DTA on the S100β-positive cell number (J) and the S100β-positive cell density (K). (**L** and **M**) Effects of DTA on the area of the GFAP-positive region (L) and the GFAP signal density (M). (**N**) Quantification of the NeuN-positive area. $^{*}P < 0.05$; $^{**}P < 0.01$. Error bars in (E) and (F) represent means ± standard error of the mean, and those in (G) and (J) to (N) represent means ± standard deviation. Scale bars, 1 mm (A, left; D, bottom), 0.5 mm (A, right; H), 4 mm (C), 2 mm (D, top), and 0.2 mm (I). D, dorsal; EP, electroporated side; Non-EP, non-electroporated side.

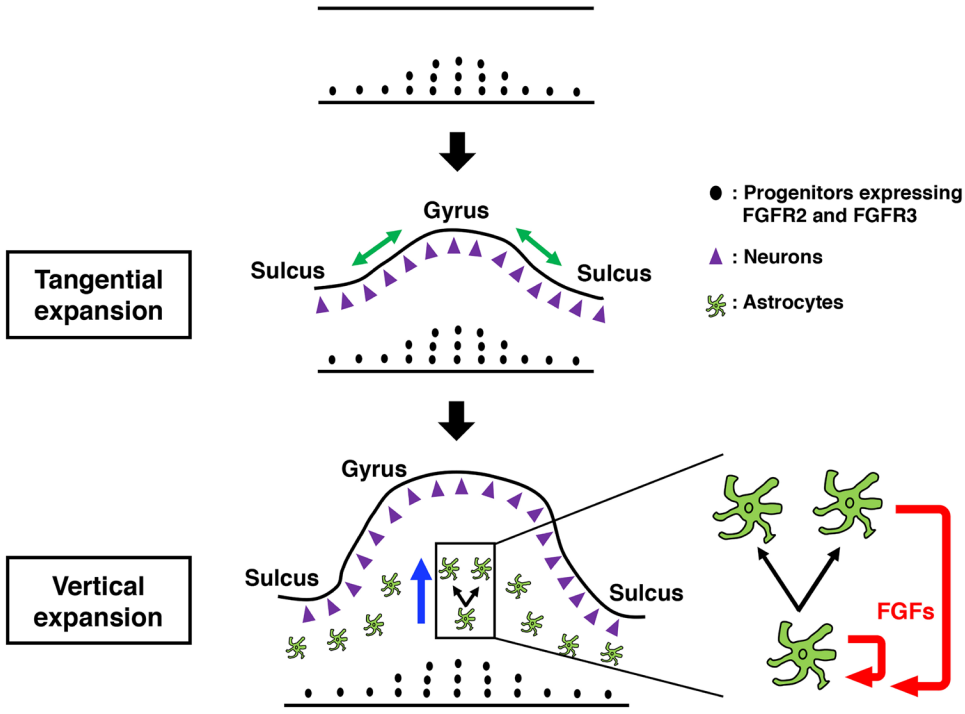

Fig. 6. Two-step model of cortical folding. Previous studies have suggested that the tangential expansion of the cortical surface is involved in cortical folding. In this study, we found that the vertical expansion of the deep pallial regions, which accompanies astrogenesis, is crucial for cortical folding. Here, we propose a two-step model involving cooperation between the tangential expansion of the cortical surface (green arrows) and the vertical expansion of the deep pallial regions (blue arrow); the tangential expansion of the cortical surface mediates the initiation of cortical folding during early development, and this is followed by the vertical expansion of the deep pallial regions mediated by astrogenesis, resulting in the development of cortical folds. Our findings suggest that a positive feedback loop driven by FGF signaling (red arrows) enables marked expansion of astrocytes in restricted areas within gyri during the vertical expansion of the deep pallial regions. We also propose that FGF signaling has dual functions related to the local generation of astrocytes in the developing cerebral cortex. First, FGF signaling controls the generation of astrocytes from SVZ progenitors by regulating the proliferation of SVZ progenitors. FGFR-positive SVZ progenitors are more abundant in prospective gyral regions. The proliferation of SVZ progenitors regulated by FGF signaling in gyri seems to be responsible for the initial abundance of astrocytes in gyri during early development. Second, our data suggest that FGF signaling induces the proliferation of differentiated astrocytes in an autocrine manner (red arrows). Therefore, it is plausible that the number of astrocytes is greatly increased in gyri of the gyrencephalic brain through a positive feedback loop driven by FGF signaling.

an initial increase in astrocytes in gyri (Fig. 6). Second, as shown in this study, a positive feedback loop driven by FGF signaling enhances the proliferation of differentiated astrocytes in an autocrine manner. We showed that activation of FGF signaling markedly increased astrocytes by promoting their proliferation and resulted in a gyrus-like structure in the mouse cerebral cortex. Therefore, we propose that increase in astrocytes resulting from a positive feedback loop driven by FGF signaling is an important mechanism of cortical folding (Fig. 6).

The number of glial cells in the mammalian brain is vastly correlated with the mass of brain structures (*13*). In this study, we found that the expression levels of *FGF1* in astrocytes are higher in ferrets than in mice. Furthermore, our results demonstrated that FGF signaling likely determines the abundance of astrocytes. Thus, our findings suggest that differences between species in expression levels of FGF ligands determine the differences in astrocyte abundance and distinguish gyrencephalic and lissencephalic brains in those species. It would be intriguing to investigate the expression levels of FGF ligands in various mammalian species.

The number of astrocytes has markedly increased in the white matter of the cerebral cortex during evolution. Because the white matter contains many myelinated axons, it seems that these astrocytes have functional interactions with myelinated axons, which connect various cortical regions and increased markedly during evolution. It was reported that astrocytes are associated with the nodes of Ranvier and are important for clearing extracellular potassium released by neuronal activity (*47*, *48*). It was also reported that perinodal astrocytes regulate myelin thickness and nodal gap length, both of which influence the conduction velocity of myelinated axons (*19*). Consistent with these findings, recent data from human neuroimaging studies demonstrated that the regulation of myelin structures in the white matter is crucial for learning and plasticity throughout life (*49*). Thus, it seems likely that increased astrocytes are crucial not only for gyrification but also for structural modifications of the whiter matter in gyrencephalic mammals.

MATERIALS AND METHODS

Animals

Normally pigmented, sable ferrets (*Mustela putorius furo*) were purchased from Marshall Farms (North Rose, NY). Ferrets were maintained as described previously (*28*). The day of conception and that of birth were counted as E0 and P0, respectively. All procedures were performed in accordance with protocols approved by the Animal Care Committee of Kanazawa University.

IUE for ferrets and mice

IUE for ferrets was performed as described previously (*28*, *30*). Briefly, the uterine horns of anesthetized pregnant ferrets were exposed and kept wet by adding drops of phosphate-buffered saline (PBS) intermittently. The location of embryos was visualized with transmitted light delivered through an optical fiber cable. Approximately 2 to 5 μl of DNA solution were injected into the lateral ventricle using a pulled glass micropipette. Each embryo within the uterus was placed between tweezer-type electrodes with a diameter of 5 mm (CUY650-P5; NEPA Gene, Japan). Square electric pulses (100 V, 50 ms) were passed five times at 1-s intervals using an electroporator (ECM830, BTX). The wall and skin of the abdominal cavity were sutured, and the embryos were allowed to develop normally. IUE for mice was performed as described previously (*50*). When wide areas needed to be transfected, the IUE procedure was repeated twice using a different electrode position each time.

Plasmids

pCAG-EGFP and pCAG-mCherry were described previously (*50*). The helper plasmid pCAG-PBase was provided by K. Woltjen (*51*), and the donor plasmid pPB-CAG-EiP was obtained from A. Hotta (*52*). After the CAG promoter and EGFP were removed from pPB-CAG-EiP, the gfa2 promoter from pgfa2-lacZ, which was provided by M. Brenner (*37*), and EGFP were inserted to make pPB-gfa2-EGFP. To make pPB-gfa2-DTA, the EGFP of pPB-gfa2-EGFP was replaced with DTA. pPB-CAG-EGFP (*53*) and pCAG-sFGFR3 (*31*) were described previously. pPB-CAG-loxP-ER^{T2}CreER^{T2}-loxP-FGF8-IRES2-EGFP was made by inserting loxP-ER^{T2}CreER^{T2}-loxP developed by M. G. Holt and FGF8-IRES2-EGFP derived from pCAG-FGF8 (*33*) and pIRES2-EGFP (Clontech) into the pPB-CAG vector. A secreted form of human FGF1 was constructed as described previously (*54*, *55*) and then inserted into the Eco RI restriction site of pPB-CAG-loxP-ER^{T2}CreER^{T2}-loxP-IRES2-EGFP to make pPB-CAG-loxP-ER^{T2}CreER^{T2}-loxP-FGF1-IRES2-EGFP. Plasmids were purified using the EndoFree Plasmid Maxi Kit (QIAGEN, Germany).

In situ hybridization

Ferrets and mice were deeply anesthetized and transcardially perfused with 4% paraformaldehyde (PFA) in PBS. Dissected brains were postfixed overnight with 4% PFA in PBS. The brains were cryoprotected by 3-day immersion in 30% sucrose in PBS and embedded in optimal cutting temperature (OCT) compound. Coronal sections of 20-μm thickness were prepared using a cryostat and pretreated with proteinase K.

RNAscope ISH was performed in accordance with the manufacturer's instructions using an RNAscope 2.5 HD detection reagent kit (Advanced Cell Diagnostics). The sections were then subjected to staining with anti-GS antibody and Hoechst 33342. A ferret *FGF1* probe (accession no. XM_004744724.2), a ferret *FGF2* probe (accession no. XM_013053919.1), a ferret *ETV5* probe (accession no. XM_004745196.2), a ferret *SPRY2* probe (accession no. XM_004754432.2), a mouse *Fgf1* probe (accession no. NM_010197.3), a mouse *Etv5* probe (accession no. NM_023794.2), a mouse *Spry2* probe (accession no. NM_011897.3), and a *dapB* probe (accession no. EF191515) were purchased from Advanced Cell Diagnostics. The *dapB* probe targeting the bacterial *dapB* gene was used as a negative control.

ISH using digoxigenin-labeled RNA probes was performed as described previously (*50*). Briefly, sections of 20-μm thickness were incubated overnight with digoxigenin-labeled RNA probes in hybridization buffer [50% formamide, 5× saline sodium citrate buffer, 5× Denhardt's solution, yeast RNA (0.3 mg/ml), herring sperm DNA (0.1 mg/ml), and 1 mM dithiothreitol]. The sections were then incubated with an alkaline phosphatase–conjugated anti-digoxigenin antibody (Roche) and were visualized using nitro blue tetrazolium/bromochloroindolyl phosphate (NBT/BCIP) as substrates. The sections were then subjected to Hoechst 33342 staining. The *PLP* probe, the *FGFR2* probe, and the *FGFR3* probe were described previously (*31*, *53*).

Immunohistochemistry

Immunohistochemistry was performed as described previously with modifications (*50*). Ferrets and mice were anesthetized and transcardially perfused with 4% PFA in PBS. Dissected brains were postfixed overnight with 4% PFA in PBS. The brains were cryoprotected by 3-day immersion in 30% sucrose in PBS and embedded in OCT compound. Coronal sections of 50-μm thickness were prepared using a cryostat, permeabilized with 0.3% Triton X-100 in PBS, and treated with 2% skim milk, 0.3% Triton X-100 in PBS. The sections were incubated overnight with primary antibodies and washed. After being incubated with Alexa Fluor 488–, Alexa Fluor 647–, and Cy3-conjugated secondary antibodies and Hoechst 33342 (1 μg/ml), the sections were washed and mounted. For the detection of biotinylated anti–red fluorescent protein (RFP) antibody, sections were incubated with streptavidin-conjugated Alexa Fluor 546. The primary antibodies included anti-GFAP antibody (Sigma-Aldrich), anti-S100β antibody (Synaptic Systems), anti-NeuN antibody (Cell Signaling), anti-GFP antibody (Medical & Biological Laboratories), anti-GFP antibody (Nacalai), anti-RFP antibody (Medical & Biological Laboratories), biotinylated anti-RFP antibody (Abcam), anti-Ctip2 antibody (Abcam), anti-Cux1 antibody (Santa Cruz Biotechnology), anti–Ki-67 antibody (Thermo Fisher Scientific), anti-Satb2 antibody (Abcam), anti-Sox9 antibody (R&D Systems), anti-Sox10 antibody (Santa Cruz Biotechnology), anti-Pax6 antibody (Covance), and anti-GS antibody (Sigma-Aldrich).

Primary culture of astrocytes

Astrocyte culture was prepared as described previously with modifications (*56*). Briefly, cerebral cortices from neonatal ferrets and mice at P1 were dissociated in Hepes-buffered saline containing Dispase II. Cells were plated on poly-D-lysine–coated flasks in Dulbecco's modified Eagle's medium (DMEM) supplemented with 10% fetal bovine serum. Ten days later, the flasks were shaken overnight, and the adherent cell population was collected. More than 96% of the collected cells were positive for GFAP, indicating that almost all of the collected cells were astrocytes.

To investigate the effects of FGF1 and FGF2, 0.5×10^5 to 0.75×10^5 astrocytes were plated on a 13-mm glass coverslip coated with poly-L-lysine in a 24-well plate. The cells were maintained in serum-free medium (50% Neurobasal medium, 50% DMEM, 1 mM sodium pyruvate, 2 mM glutamine, and 1× B27 supplement) for 1 day. Then, FGF1 protein (R&D Systems, 232-FA) or FGF2 protein (R&D Systems, 233-FB) was added at a concentration of 10 ng/ml. After 24 hours, the cells were fixed with 4% PFA.

To test the roles of endogenous FGF ligands secreted from astrocytes, 1.5×10^5 to 2.5×10^5 astrocytes were plated in each well of a 24-well plate and maintained in the serum-free medium described above for 1 day. Then, BGJ398 (ChemieTek, CT-BGJ398) was added

at indicated concentrations. After 24 hours, the cells were fixed with 4% PFA.

RNA-seq transcriptome profiling

Total RNAs from cultured ferret and mouse astrocytes were used for RNA library preparation using the TruSeq Stranded mRNA Sample Preparation Kit (Illumina), with polyA selection for ribosomal RNA depletion. The RNA-seq libraries were generated in duplicate from 500 ng of total RNAs extracted from cultured ferret or mouse astrocytes. The libraries were sequenced on Illumina HiSeq 2000 to obtain paired-end 101–base pair reads for each sample.

RNA-seq reads from ferret and mouse cultured astrocytes were aligned to their reference genomes using STAR v2.7.0f (*57*). The Ensembl reference genomes used were as follows: ferret, MusPutFur1.0.99; mouse, GRCm38.99 (*58*). The gene expression profiles were quantified using Cufflinks v2.2.1 (*59*) from the aligned RNA-seq reads with gene annotation information corresponding to each of the above reference genomes. Gene expression levels were given by fragments per kilobase of transcript per million mapped reads (FPKM), which is normalized by the number of RNA fragments mapped to the reference genome and the total length of all exons in the transcript.

Microscopy

Epifluorescence microscopy was performed with BZ-9000 and BZ-X710 microscopes (Keyence). Confocal microscopy was performed with an inverted Nikon Eclipse Ti2 confocal microscope (Nikon).

Injections of FGF1 and FGF2 proteins into the lateral ventricle of newborn mouse pups

FGF1 protein (R&D Systems, 232-FA) or FGF2 protein (R&D Systems, 233-FB) was dissolved in PBS at a concentration of 100 ng/μl. Approximately 2 to 3 μl of the protein solution or vehicle were injected into the lateral ventricle of anesthetized mice daily from P3 to P5, and the brains were dissected at P6.

AGN 193109 treatment

AGN 193109 has been widely used to inhibit RA signaling in vivo *(60)*. AGN 193109 (Toronto Research Chemicals) was dissolved in dimethyl sulfoxide (Sigma-Aldrich) at a concentration of 4 mg/ml as a stock solution. The stock solution was diluted with dimethyl sulfoxide to appropriate concentrations and mixed with sesame oil in a proportion of 1:1 by volume. AGN 193109 (1 μg/g of body weight) or vehicle was subcutaneously injected into ferrets from P3 to P15 daily, and the brains were dissected at P16.

4-Hydroxytamoxifen treatment

4-Hydroxytamoxifen (4-OHT) (Sigma-Aldrich) administration was performed as described previously (*50*). Briefly, 4-OHT was dissolved in 99.5% ethanol at a concentration of 20 mg/ml and diluted with sesame oil at a concentration of 2 mg/ml before use. After the ethanol was vaporized, 4-OHT (66 μg/g of body weight) in sesame oil was injected subcutaneously into mouse pups at P0, P1, and P2.

Quantification of vertical expansion in gyri

Thicknesses of the CP and the SP-OSVZ were measured at the gyral crown of the SSG and at the sulcal bottoms of the LS and the SSS using coronal sections of the ferret cerebral cortex at P6, P10, and P16. The border of each stratum was defined using Hoechst images. Thicknesses were measured using a BZ-II analysis system (Keyence).

Vertical expansion was defined as follows: the thickness in the SSG minus that in the LS or the SSS. To minimize the variation of the vertical expansion values depending on the positions of coronal sections in electroporated brains, the vertical expansion value on the electroporated side was divided by the corresponding value on the contralateral control side to give the vertical expansion ratio.

Quantification of the local GYS ratio and the local SD ratio

Quantification of the local GYS ratio and the local SD ratio was performed as described previously (*30*). Briefly, serial coronal sections of 50-μm thickness containing electroporated areas were prepared. The serial sections were stained with Hoechst 33342, and tiling images of whole sections were acquired using a BZ-9000 microscope (Keyence). We then measured the sizes of gyri (local GYS) and the depths of sulci (local SD) using a BZ-II analysis system (Keyence). To minimize variation of the local GYS values and the local SD values depending on the positions of coronal sections in the brain, the local GYS value and the local SD value on the electroporated side were divided by corresponding values on the contralateral control side to give the local GYS ratio and the local SD ratio, respectively. The averages of the local GYS ratio and the local SD ratio were calculated using three sections for each animal. The local GYS ratio and the local SD ratio would be zero if cortical folding was completely blocked by genetic manipulations.

Quantification of the local GYS value and the local SD value

Coronal sections containing the SSG were prepared. Sections were selected every 0.1 mm, and serial sections were stained with Hoechst 33342. The averages of the size of the gyrus (local GYS) for the SSG and the depth of the sulcus (local SD) for the LS were calculated using three serial sections for each animal.

Quantification of S100β, GFAP, and NeuN signals

Coronal sections of ferret brains were stained with anti-GFAP, anti-S100β, or anti-NeuN antibody and Hoechst 33342. Anti-GFAP antibody preferentially detects astrocytes in the white matter, while anti-S100β antibody detects astrocytes in both the white matter and the gray matter. To remove background signals, the average signal intensity of negative cells was subtracted. Hoechst 33342– and S100β–double-positive areas were determined to be S100β-positive nuclei, and the number of these nuclei was counted using the "Analyze Particles" tool of ImageJ software. GFAP- and NeuN-positive areas were measured using ImageJ software. For quantifications using electroporated brains (Figs. 2, 3, and 5 and figs. S1 and S6), to minimize variation of measured values resulting from differences in the positions of coronal sections in the brain, the value on the electroporated side was divided by that on the contralateral side. The ratios were then compared between control and experimental brains. For quantifications of AGN 193109 experiments (Fig. 4), coronal sections at similar anteroposterior levels were used for control and AGN 193109 samples.

Quantification of *FGF1*, *ETV5*, and *SPRY2* signals

We investigated the expression of *FGF1*, *ETV5*, and *SPRY2* in the ferret cortex at P36 and the mouse cortex at P18 because the developmental processes of the ferret cortex at P36 approximately correspond to those occurring in the mouse cortex at P18. Sections were

subjected to RNAscope ISH, GS immunohistochemistry, and Hoechst 33342 staining. A series of *z*-stack images were acquired with a BZ-X710 microscope and processed with the full focus function of BZ-II Analyzer software (Keyence). Astrocytes in the SP/IZ of the cerebral cortex were randomly selected, and the numbers of *FGF1*, *ETV5*, and *SPRY2* puncta in each astrocyte were counted. The averages of the numbers of *FGF1*, *ETV5*, and *SPRY2* puncta were calculated from more than 20 astrocytes for each animal. Calculation of the H-score was performed according to the manufacturer's procedure (Advanced Cell Diagnostics). Briefly, the numbers of *FGF1*, *ETV5*, and *SPRY2* puncta were binned into five groups based on the number of dots per cell as follows: bin 0 = 0 dots per cell, bin 1 = 1 to 3 dots per cell, bin 2 = 4 to 9 dots per cell, bin 3 = 10 to 15 dots per cell, and bin 4 = >15 dots per cell. The H-score was calculated as follows:

H-score = (0 × (% of cells in bin 0)) + (1 × (% of cells in bin 1)) + (2 × (% of cells in bin 2)) + (3 × (% of cells in bin 3)) + (4 × (% of cells in bin 4)).

Quantification of the vertical expansion of the mouse cortex by the activation of FGF signaling

Cortical thickness was measured at the end points and the middle point of mCherry-positive transfected regions, and the thickness at the middle point was divided by the average of the thicknesses at both ends.

Expression analysis of *Fgf* ligands in the mouse cerebral cortex

Expression levels of *Fgf* ligands in various types of cells in the mouse cerebral cortex were analyzed using a transcriptome dataset (www.brainrnaseq.org). The public datasets include neurons, astrocytes, and endothelial cells from P7 cerebral cortex and oligodendrocyte-lineage cells from P17 cerebral cortex.

Statistics

Sample sizes, statistical tests, and statistical significances were described in the figure legends and Results. All *n* values indicate the numbers of animals. A two-tailed Welch's *t* test was used unless otherwise mentioned. No statistical methods were used to predetermine sample sizes. The sample sizes were chosen based on published studies and current standards in the field. In figures, asterisks indicate statistical significance: $^{*}P < 0.05$ and $^{**}P < 0.01$.

SUPPLEMENTARY MATERIALS

Supplementary material for this article is available at https://science.org/doi/10.1126/sciadv.abi5209

View/request a protocol for this paper from *Bio-protocol*.

REFERENCES AND NOTES

1. N. Kalebic, W. B. Huttner, Basal progenitor morphology and neocortex evolution. *Trends Neurosci.* **43**, 843–853 (2020).
2. C. Llinares-Benadero, V. Borrell, Deconstructing cortical folding: Genetic, cellular and mechanical determinants. *Nat. Rev. Neurosci.* **20**, 161–176 (2019).
3. J. H. Lui, D. V. Hansen, A. R. Kriegstein, Development and evolution of the human neocortex. *Cell* **146**, 18–36 (2011).
4. Z. Molnar, G. J. Clowry, N. Sestan, A. Alzu'bi, T. Bakken, R. F. Hevner, P. S. Huppi, I. Kostovic, P. Rakic, E. S. Anton, D. Edwards, P. Garcez, A. Hoerder-Suabedissen, A. Kriegstein, New insights into the development of the human cerebral cortex. *J. Anat.* **235**, 432–451 (2019).
5. Z. Molnar, C. Metin, A. Stoykova, V. Tarabykin, D. J. Price, F. Francis, G. Meyer, C. Dehay, H. Kennedy, Comparative aspects of cerebral cortical development. *Eur. J. Neurosci.* **23**, 921–934 (2006).
6. P. Rakic, Evolution of the neocortex: A perspective from developmental biology. *Nat. Rev. Neurosci.* **10**, 724–735 (2009).
7. T. Sun, R. F. Hevner, Growth and folding of the mammalian cerebral cortex: From molecules to malformations. *Nat. Rev. Neurosci.* **15**, 217–232 (2014).
8. A. J. Barkovich, R. Guerrini, R. I. Kuzniecky, G. D. Jackson, W. B. Dobyns, A developmental and genetic classification for malformations of cortical development: Update 2012. *Brain* **135**, 1348–1369 (2012).
9. F. Francis, G. Meyer, C. Fallet-Bianco, S. Moreno, C. Kappeler, A. C. Socorro, F. P. Tuy, C. Beldjord, J. Chelly, Human disorders of cortical development: From past to present. *Eur. J. Neurosci.* **23**, 877–893 (2006).
10. R. Guerrini, C. Marini, Genetic malformations of cortical development. *Exp. Brain Res.* **173**, 322–333 (2006).
11. A. Poduri, G. D. Evrony, X. Cai, C. A. Walsh, Somatic mutation, genomic variation, and neurological disease. *Science* **341**, 1237758 (2013).
12. M. E. Ross, C. A. Walsh, Human brain malformations and their lessons for neuronal migration. *Annu. Rev. Neurosci.* **24**, 1041–1070 (2001).
13. S. Herculano-Houzel, The glia/neuron ratio: How it varies uniformly across brain structures and species and what that means for brain physiology and evolution. *Glia* **62**, 1377–1391 (2014).
14. N. J. Allen, C. Eroglu, Cell biology of astrocyte-synapse interactions. *Neuron* **96**, 697–708 (2017).
15. A. M. Brown, B. R. Ransom, Astrocyte glycogen and brain energy metabolism. *Glia* **55**, 1263–1271 (2007).
16. W. S. Chung, N. J. Allen, C. Eroglu, Astrocytes control synapse formation, function, and elimination. *Cold Spring Harb. Perspect. Biol.* **7**, a020370 (2015).
17. L. Pellerin, How astrocytes feed hungry neurons. *Mol. Neurobiol.* **32**, 59–72 (2005).
18. M. Simard, M. Nedergaard, The neurobiology of glia in the context of water and ion homeostasis. *Neuroscience* **129**, 877–896 (2004).
19. D. J. Dutta, D. H. Woo, P. R. Lee, S. Pajevic, O. Bukalo, W. C. Huffman, H. Wake, P. J. Basser, S. SheikhBahaei, V. Lazarevic, J. C. Smith, R. D. Fields, Regulation of myelin structure and conduction velocity by perinodal astrocytes. *Proc. Natl. Acad. Sci. U.S.A.* **115**, 11832–11837 (2018).
20. A. V. Molofsky, R. Krencik, E. M. Ullian, H. H. Tsai, B. Deneen, W. D. Richardson, B. A. Barres, D. H. Rowitch, Astrocytes and disease: A neurodevelopmental perspective. *Genes Dev.* **26**, 891–907 (2012).
21. X. Han, M. Chen, F. Wang, M. Windrem, S. Wang, S. Shanz, Q. Xu, N. A. Oberheim, L. Bekar, S. Betstadt, A. J. Silva, T. Takano, S. A. Goldman, M. Nedergaard, Forebrain engraftment by human glial progenitor cells enhances synaptic plasticity and learning in adult mice. *Cell Stem Cell* **12**, 342–353 (2013).
22. D. Del Toro, T. Ruff, E. Cederfjall, A. Villalba, G. Seyit-Bremer, V. Borrell, R. Klein, Regulation of cerebral cortex folding by controlling neuronal migration via FLRT adhesion molecules. *Cell* **169**, 621–635.e16 (2017).
23. S. A. Fietz, I. Kelava, J. Vogt, M. Wilsch-Brauninger, D. Stenzel, J. L. Fish, D. Corbeil, A. Riehn, W. Distler, R. Nitsch, W. B. Huttner, OSVZ progenitors of human and ferret neocortex are epithelial-like and expand by integrin signaling. *Nat. Neurosci.* **13**, 690–699 (2010).
24. M. B. Johnson, P. P. Wang, K. D. Atabay, E. A. Murphy, R. N. Doan, J. L. Hecht, C. A. Walsh, Single-cell analysis reveals transcriptional heterogeneity of neural progenitors in human cortex. *Nat. Neurosci.* **18**, 637–646 (2015).
25. N. Kalebic, C. Gilardi, B. Stepien, M. Wilsch-Brauninger, K. R. Long, T. Namba, M. Florio, B. Langen, B. Lombardot, A. Shevchenko, M. W. Kilimann, H. Kawasaki, P. Wimberger, W. B. Huttner, Neocortical expansion due to increased proliferation of basal progenitors is linked to changes in their morphology. *Cell Stem Cell* **24**, 535–550.e9 (2019).
26. R. S. Smith, C. J. Kenny, V. Ganesh, A. Jang, R. Borges-Monroy, J. N. Partlow, R. S. Hill, T. Shin, A. Y. Chen, R. N. Doan, A. K. Anttonen, J. Ignatius, L. Medne, C. G. Bonnemann, J. L. Hecht, O. Salonen, A. J. Barkovich, A. Poduri, M. Wilke, M. C. Y. de Wit, G. M. S. Mancini, L. Sztriha, K. Im, D. Amrom, E. Andermann, R. Paetau, A. E. Lehesjoki, C. A. Walsh, M. K. Lehtinen, Sodium channel SCN3A (NaV1.3) regulation of human cerebral cortical folding and oral motor development. *Neuron* **99**, 905–913.e7 (2018).
27. M. B. Johnson, X. Sun, A. Kodani, R. Borges-Monroy, K. M. Girskis, S. C. Ryu, P. P. Wang, K. Patel, D. M. Gonzalez, Y. M. Woo, Z. Yan, B. Liang, R. S. Smith, M. Chatterjee, D. Coman, X. Papademetris, L. H. Staib, F. Hyder, J. B. Mandeville, P. E. Grant, K. Im, H. Kwak, J. F. Engelhardt, C. A. Walsh, B. I. Bae, Aspm knockout ferret reveals an evolutionary mechanism governing cerebral cortical size. *Nature* **556**, 370–375 (2018).
28. H. Kawasaki, L. Iwai, K. Tanno, Rapid and efficient genetic manipulation of gyrencephalic carnivores using in utero electroporation. *Mol. Brain* **5**, 24 (2012).
29. Z. Kou, Q. Wu, X. Kou, C. Yin, H. Wang, Z. Zuo, Y. Zhuo, A. Chen, S. Gao, X. Wang, CRISPR/Cas9-mediated genome engineering of the ferret. *Cell Res.* **25**, 1372–1375 (2015).
30. Y. Shinmyo, Y. Terashita, T. A. Dinh Duong, T. Horiike, M. Kawasumi, K. Hosomichi, A. Tajima, H. Kawasaki, Folding of the cerebral cortex requires Cdk5 in upper-layer neurons in gyrencephalic mammals. *Cell Rep.* **20**, 2131–2143 (2017).

31. N. Matsumoto, Y. Shinmyo, Y. Ichikawa, H. Kawasaki, Gyrification of the cerebral cortex requires FGF signaling in the mammalian brain. *eLife* **6**, e29285 (2017).
32. M. Nonaka-Kinoshita, I. Reillo, B. Artegiani, M. A. Martinez-Martinez, M. Nelson, V. Borrell, F. Calegari, Regulation of cerebral cortex size and folding by expansion of basal progenitors. *EMBO J.* **32**, 1817–1828 (2013).
33. K. Masuda, T. Toda, Y. Shinmyo, H. Ebisu, Y. Hoshiba, M. Wakimoto, Y. Ichikawa, H. Kawasaki, Pathophysiological analyses of cortical malformation using gyrencephalic mammals. *Sci. Rep.* **5**, 15370 (2015).
34. Y. Zhang, K. Chen, S. A. Sloan, M. L. Bennett, A. R. Scholze, S. O'Keeffe, H. P. Phatnani, P. Guarnieri, C. Caneda, N. Ruderisch, S. Deng, S. A. Liddelow, C. Zhang, R. Daneman, T. Maniatis, B. A. Barres, J. Q. Wu, An RNA-sequencing transcriptome and splicing database of glia, neurons, and vascular cells of the cerebral cortex. *J. Neurosci.* **34**, 11929–11947 (2014).
35. B. G. Rash, A. Duque, Y. M. Morozov, J. I. Arellano, N. Micali, P. Rakic, Gliogenesis in the outer subventricular zone promotes enlargement and gyrification of the primate cerebrum. *Proc. Natl. Acad. Sci. U.S.A.* **116**, 7089–7094 (2019).
36. H. Asano, M. Aonuma, T. Sanosaka, J. Kohyama, M. Namihira, K. Nakashima, Astrocyte differentiation of neural precursor cells is enhanced by retinoic acid through a change in epigenetic modification. *Stem Cells* **27**, 2744–2752 (2009).
37. Y. Lee, A. Messing, M. Su, M. Brenner, GFAP promoter elements required for region-specific and astrocyte-specific expression. *Glia* **56**, 481–493 (2008).
38. C. Dehay, H. Kennedy, K. S. Kosik, The outer subventricular zone and primate-specific cortical complexification. *Neuron* **85**, 683–694 (2015).
39. D. V. Hansen, J. H. Lui, P. R. Parker, A. R. Kriegstein, Neurogenic radial glia in the outer subventricular zone of human neocortex. *Nature* **464**, 554–561 (2010).
40. A. Kriegstein, S. Noctor, V. Martinez-Cerdeno, Patterns of neural stem and progenitor cell division may underlie evolutionary cortical expansion. *Nat. Rev. Neurosci.* **7**, 883–890 (2006).
41. V. Martinez-Cerdeno, S. C. Noctor, A. R. Kriegstein, The role of intermediate progenitor cells in the evolutionary expansion of the cerebral cortex. *Cereb. Cortex* **16**, i152–i161 (2006).
42. I. Reillo, V. Borrell, Germinal zones in the developing cerebral cortex of ferret: Ontogeny, cell cycle kinetics, and diversity of progenitors. *Cereb. Cortex* **22**, 2039–2054 (2012).
43. M. Heide, C. Haffner, A. Murayama, Y. Kurotaki, H. Shinohara, H. Okano, E. Sasaki, W. B. Huttner, Human-specific ARHGAP11B increases size and folding of primate neocortex in the fetal marmoset. *Science* **369**, 546–550 (2020).
44. C. C. Gertz, A. R. Kriegstein, Neuronal migration dynamics in the developing ferret cortex. *J. Neurosci.* **35**, 14307–14315 (2015).
45. I. Reillo, C. de Juan Romero, M. A. Garcia-Cabezas, V. Borrell, A role for intermediate radial glia in the tangential expansion of the mammalian cerebral cortex. *Cereb. Cortex* **21**, 1674–1694 (2011).
46. I. H. Smart, C. Dehay, P. Giroud, M. Berland, H. Kennedy, Unique morphological features of the proliferative zones and postmitotic compartments of the neural epithelium giving rise to striate and extrastriate cortex in the monkey. *Cereb. Cortex* **12**, 37–53 (2002).
47. H. K. Kimelberg, Functions of mature mammalian astrocytes: A current view. *Neuroscientist* **16**, 79–106 (2010).
48. D. R. Serwanski, P. Jukkola, A. Nishiyama, Heterogeneity of astrocyte and NG2 cell insertion at the node of ranvier. *J. Comp. Neurol.* **525**, 535–552 (2017).
49. C. Sampaio-Baptista, H. Johansen-Berg, White matter plasticity in the adult brain. *Neuron* **96**, 1239–1251 (2017).
50. M. Wakimoto, K. Sehara, H. Ebisu, Y. Hoshiba, S. Tsunoda, Y. Ichikawa, H. Kawasaki, Classic cadherins mediate selective intracortical circuit formation in the mouse neocortex. *Cereb. Cortex* **25**, 3535–3546 (2015).
51. S. I. Kim, F. Oceguera-Yanez, C. Sakurai, M. Nakagawa, S. Yamanaka, K. Woltjen, Inducible transgene expression in human iPS cells using versatile all-in-one piggyBac transposons. *Methods Mol. Biol.* **1357**, 111–131 (2016).
52. H. Matsui, N. Fujimoto, N. Sasakawa, Y. Ohinata, M. Shima, S. Yamanaka, M. Sugimoto, A. Hotta, Delivery of full-length factor VIII using a piggyBac transposon vector to correct a mouse model of hemophilia A. *PLOS ONE* **9**, e104957 (2014).
53. T. Hamabe-Horiike, K. Kawasaki, M. Sakashita, C. Ishizu, T. Yoshizaki, S. I. Harada, K. Ogawa-Ochiai, Y. Shinmyo, H. Kawasaki, Glial cell type-specific gene expression in the mouse cerebrum using the piggyBac system and in utero electroporation. *Sci. Rep.* **11**, 4864 (2021).
54. R. Forough, Z. Xi, M. MacPhee, S. Friedman, K. A. Engleka, T. Sayers, R. H. Wiltrout, T. Maciag, Differential transforming abilities of non-secreted and secreted forms of human fibroblast growth factor-1. *J. Biol. Chem.* **268**, 2960–2968 (1993).
55. E. G. Nabel, Z. Y. Yang, G. Plautz, R. Forough, X. Zhan, C. C. Haudenschild, T. Maciag, G. J. Nabel, Recombinant fibroblast growth factor-1 promotes intimal hyperplasia and angiogenesis in arteries in vivo. *Nature* **362**, 844–846 (1993).
56. T. Hattori, M. Kaji, H. Ishii, R. Jureepon, M. Takarada-Iemata, H. Minh Ta, T. M. Le, A. Konno, H. Hirai, Y. Shiraishi, N. Ozaki, Y. Yamamoto, H. Okamoto, S. Yokoyama, H. Higashida, Y. Kitao, O. Hori, CD38 positively regulates postnatal development of astrocytes cell-autonomously and oligodendrocytes non-cell-autonomously. *Glia* **65**, 974–989 (2017).
57. A. Dobin, C. A. Davis, F. Schlesinger, J. Drenkow, C. Zaleski, S. Jha, P. Batut, M. Chaisson, T. R. Gingeras, STAR: Ultrafast universal RNA-seq aligner. *Bioinformatics* **29**, 15–21 (2013).
58. F. Cunningham, P. Achuthan, W. Akanni, J. Allen, M. R. Amode, I. M. Armean, R. Bennett, J. Bhai, K. Billis, S. Boddu, C. Cummins, C. Davidson, K. J. Dodiya, A. Gall, C. G. Giron, L. Gil, T. Grego, L. Haggerty, E. Haskell, T. Hourlier, O. G. Izuogu, S. H. Janacek, T. Juettemann, M. Kay, M. R. Laird, I. Lavidas, Z. Liu, J. E. Loveland, J. C. Marugan, T. Maurel, A. C. McMahon, B. Moore, J. Morales, J. M. Mudge, M. Nuhn, D. Ogeh, A. Parker, A. Parton, M. Patricio, A. I. Abdul Salam, B. M. Schmitt, H. Schuilenburg, D. Sheppard, H. Sparrow, E. Stapleton, M. Szuba, K. Taylor, G. Threadgold, A. Thormann, A. Vullo, B. Walts, A. Winterbottom, A. Zadissa, M. Chakiachvili, A. Frankish, S. E. Hunt, M. Kostadima, N. Langridge, F. J. Martin, M. Muffato, E. Perry, M. Ruffier, D. M. Staines, S. J. Trevanion, B. L. Aken, A. D. Yates, D. R. Zerbino, P. Flicek, Ensembl 2019. *Nucleic Acids Res.* **47**, D745–D751 (2019).
59. C. Trapnell, D. G. Hendrickson, M. Sauvageau, L. Goff, J. L. Rinn, L. Pachter, Differential analysis of gene regulation at transcript resolution with RNA-seq. *Nat. Biotechnol.* **31**, 46–53 (2013).
60. N. Etchamendy, V. Enderlin, A. Marighetto, R. M. Vouimba, V. Pallet, R. Jaffard, P. Higueret, Alleviation of a selective age-related relational memory deficit in mice by pharmacologically induced normalization of brain retinoid signaling. *J. Neurosci.* **21**, 6423–6429 (2001).

Acknowledgments: We thank C. Yokoyama, Z. Blalock, and the Kawasaki laboratory members for critical discussions and comments on this manuscript. We also thank K. Woltjen, A. Hotta, and M. Brenner for plasmids. **Funding:** This work was supported by Grant-in-Aid for Scientific Research from the Ministry of Education, Culture, Sports, Science and Technology (MEXT); Takeda Science Foundation; the Uehara Memorial Foundation; the Naito Foundation; European Research Council (ERC) Starting Grant 281961 AstroFunc; European Commission Horizon 2020 Action NCBio 951923; European Commission FP7-PEOPLE-2012-IEF 331018 PlasticAstros; Kanazawa University SAKIGAKE Project 2018; and Kanazawa University CHOZEN Project. **Author contributions:** Y.S. and H.K. designed the experiments. Y.S., K.S., T.H.-H., N.K., A.A., K.K., T.A.D.D., M.Sa., J.R., T.H., T.K., K.H., M.Sl., M.G.H., A.T., and O.H. collected the data. Y.S. and H.K. wrote the manuscript. **Competing interests:** The authors declare that they have no competing interests. **Data and materials availability:** All data needed to evaluate the conclusions in the paper are present in the paper and/or the Supplementary Materials.

Submitted 16 March 2021
Accepted 19 January 2022
Published 11 March 2022
10.1126/sciadv.abi5209